ELSEVIER

Microporous Materials 12 (1997) 93–106

MICROPOROUS
MATERIALS

Monitoring of the structure of siliceous mesoporous molecular sieves tailored using different synthesis conditions

Michal Kruk [a], Mietek Jaroniec [a,*], Ryong Ryoo [b], Ji Man Kim [b]

[a] *Department of Chemistry, Kent State University, Kent, OH 44240, USA*
[b] *Department of Chemistry and Center for Molecular Science, Korea Advanced Institute of Science and Technology, Taeduk Science Town, Taejon, 305-701, South Korea*

Received 19 April 1997; accepted 8 July 1997

Abstract

The hexagonally ordered siliceous mesoporous molecular sieve MCM-41 and the disordered mesoporous molecular sieve designated as KIT-1 were studied by means of the X-ray diffraction (XRD), transmission electron microscopy and low temperature nitrogen adsorption over a wide pressure range. It was shown that the combination of these techniques allows for a thorough characterization of novel mesoporous materials. A repeated pH adjustment happens to be crucial in the synthesis of MCM-41 samples of high pore size uniformity. An additional influence of the salt effect (i.e. the addition of Na_4EDTA during the hydrothermal crystallization) allows one to obtain MCM-41 materials of excellent porous structures and remarkably high thermal and hydrothermal stability. The latter features may be a result of the presence of relatively thick pore walls for those mesoporous molecular sieves.

A disordered character of KIT-1, which was synthesized with an addition of Na_4EDTA to the initial synthesis gel, was supported by the fact that the sample exhibits a high pore size uniformity but yet a rather featureless XRD pattern. It was shown that comparative methods, such as the α_s-plot, are very useful for analysis of mesoporous molecular sieves, allowing for an accurate calculation of the specific surface area of the samples, which exhibit condensation in mesopores in the pressure range used in the standard BET method. A method to calculate the pore diameter for MCM-41 samples from XRD and adsorption data was shown to be convenient and useful for an accurate pore size assessment. © 1997 Elsevier Science B.V.

Keywords: MCM-41 molecular sieve; Disordered molecular sieve; Nitrogen adsorption; Mesoporous structure characterization; Imaging of nanoporous channels

1. Introduction

After the scientists from Mobil Research and Development Corporation discovered M41S mesoporous molecular sieves [1,2], a significant effort has been made in order to understand their structure and formation mechanism, improve their structural properties and develop new materials of similar structure. The account of this work can be found in numerous recent articles (see Refs. [3–8], and the reviews in Refs. [9–11] and references cited therein). The synthesis of the M41S materials was shown to proceed via a liquid crystal templat-

* Corresponding author. Tel: +1 330 6723790; Fax: +1 330 6723816; e-mail: jaroniec@kentvm.kent.edu

PII S0927-6513(97)00060-6

ing mechanism, originally proposed by the researchers from Mobil [1,2]. It happens that M41S materials can be formed in a variety of synthesis conditions and using different surfactants as templates (see Refs. [4–11] and references cited therein). Moreover, significantly different synthesis procedures may lead to structurally similar products. However, details of structure and stability of the obtained materials are highly dependent on the synthesis procedure (see for example Refs. [6,8,12–17]). Therefore, numerous analytical techniques (such as X-ray diffraction (XRD), transmission and scanning electron microscopy, nuclear magnetic resonance spectroscopy and adsorption) have been employed to monitor the synthesis and to characterize structures of ordered mesoporous materials (see Ref. [10] and references cited therein). Among those methods, adsorption measurements appeared to be especially useful, providing information about the specific surface area, the pore size and uniformity, the pore volume, the surface and textural properties of mesoporous molecular sieves [18–23].

In the current study, mesoporous molecular sieves were obtained using sodium silicate and hexadecyltrimethylammonium chloride (HTACl) and subsequently characterized using low temperature nitrogen adsorption, XRD and transmission electron microscopy (TEM). The structure of the samples was tailored using the pH adjustment [13] and the salt effect during either the initial gelation [14,15] or the post-synthesis hydrothermal treatment [16]. It was shown that the pH adjustment procedure significantly increases the uniformity of porous structures of the materials. A further improvement of properties of MCM-41 materials was attained by employing the salt effect during the post-synthesis hydrothermal treatment. The latter effect causes a decrease in the surface area, but improves uniformity of porous structures and increases the pore wall thickness, which may be the reason of enhanced thermal and hydrothermal stability [16] of the resulting materials. Moreover, the synthesis procedure was shown to be highly reproducible.

The addition of organic salts at an initial stage of the synthesis allowed one to obtain a disordered molecular sieve designated as KIT-1, which was previously shown to exhibit a worm-like disordered three-dimensional porous structure and a remarkably high thermal and hydrothermal stability [14,15,17]. It seems that nitrogen adsorption properties of KIT-1 are very similar to those of the MCM-41 materials. The molecular sieves under study were shown to contain no noticeable amount of micropores. Surface properties of the materials (assessed from the nitrogen adsorption) were compared with those of mesoporous silica gels. High similarity of the surface properties of these two groups of materials was clearly demonstrated. Concluding, nitrogen adsorption measurements were shown to allow for detailed characterization of structural and surface properties of novel ordered and disordered molecular sieves. It needs to be noted that the mechanism of the influence of the pH adjustment and the salt effect on the structure of the materials under study is still not well-understood, although some suggestions were made previously [14–16].

2. Experimental

2.1. Materials

The synthesis procedures used in the current study were reported elsewhere [12–14,16,17]. All samples were synthesized using sodium silicate and HTACl. In the case of all MCM-41 samples, the molar composition of the initial gel mixtures was $4SiO_2 : 1HTACl : 1Na_2O : 0.15(NH_4)_2O : 200H_2O$. The sodium silicate solution (9 wt% SiO_2, Na/Si = 0.5) was prepared using 1 M NaOH solution and a colloidal silica Ludox HS40 (DuPont), as described in Refs. [12,13]. Subsequently, the sodium silicate solution was added to the HTACl solution (25 wt% HTACl) containing ammonia (NH_3/HTACl = 0.3), dropwise with vigorous stirring at room temperature. The reaction mixture was heated to 373 K. The sample #1 was heated at 373 K for 4 days without pH adjustment. In the case of the sample #2, before heating to 373 K, a small amount of acetic acid was introduced in order to adjust the pH of the reaction mixture to 10. Then, the mixture obtained was heated at 373 K for 4 days. In the

case of the sample #3, the pH of the reaction mixture was adjusted with acetic acid to 10 three times during hydrothermal synthesis, in order to improve the long-range structural order and textural uniformity of the resulting MCM-41 sample [12,13]. The samples #4B and #4A1 were synthesized in a similar way to the #3 sample, but in the case of the former samples, ethylenediaminetetraacetic acid tetrasodium salt (Na_4EDTA) was added to the reaction mixture at room temperature, after the first pH adjustment, and the mixtures were subsequently heating at 373 K for 1 day. The ratios of Na_4EDTA/HTA in the reaction mixtures were 4 and 8 for the samples #4B and #4A1 respectively. The resulting mixtures were heated again for 1 day at 373 K before the second pH adjustment. The precipitated products were filtered, washed with doubly distilled water, dried in an oven at 373 K and subsequently calcined in air under static conditions using a muffle furnace. The calcination temperature was increased from room temperature to 813 K over 10 h and maintained at 813 K for an additional 10 h.

As was already reported, the quality and the hydrothermal stability of the samples in boiling water changes in the following order: #4A1 > #4B > #3 > #2 > #1. The hydrothermal stability of the MCM-41 sample was improved remarkably by adding salts during the hydrothermal reaction [16]. Note that the sample #4A2 was synthesized in the identical way as #4A1, but they were taken from different batches.

The synthesis procedure of the KIT-1 sample was similar to that of the MCM-41 using the repeated pH adjustment, but Na_4EDTA was added to the surfactant solution before mixing with the silica source to obtain the following gel composition: $4SiO_2 : 1HTACl : 4Na_4EDTA : 1Na_2O : 0.15 (NH_4)_2O : 300H_2O$. The details of the synthesis procedure for the KIT-1 sample were described elsewhere [14,17].

2.2. Measurements

XRD spectra were recorded on a Rigaku D/MAX-III (3 kW) instrument with a Cu Kα X-ray source. TEM images were obtained from thin edges of the sample particles (< 1 μm) with a CM 20 (Philips) apparatus operating at 100 keV. Nitrogen adsorption measurements were carried out at temperature of 77 K in a relative press ure range from 10^{-6} to 0.995 using an ASAP 2010 volumetric adsorption instrument from Micromeritics (Norcross, GA). Before the measurements, the samples were degassed for 2 h at 413 K in the degas port of the adsorption apparatus.

2.3. Characterization methods

The local structure of the channel arrangement in mesoporous molecular sieves was probed using TEM images of nanosize Pt wires which fill the channels in a locally controlled manner as reported recently [15,17]. Calcined MCM-41 and KIT-1 samples were slurried in 5×10^{-5} M aqueous solutions of $Pt(NH_3)_4(NO_3)_2$ (Aldrich) for 1 h at room temperature. The solution to sample ratio was 100 ml g^{-1}. The samples were then filtered, washed with doubly distilled water and dried in a vacuum oven at 320 K. During these treatments, $Pt(NH_3)_4^{2+}$ ions corresponding to 0.1 wt% Pt were incorporated on the molecular sieves by ion exchange with protons of silanol groups. The ion-exchanged Pt species was activated by heating to 593 K in an O_2 flow. The gas flow rate was 1 l min^{-1} g^{-1}. The heating temperature was increased linearly from room temperature to 593 K over 12 h and then maintained at 593 K for 2 h. After the activation treatment was over, the O_2 gas was evacuated from the reactor at 573 K. Subsequently, the Pt species was reduced with heating in an H_2 flow. The H_2 flow rate for the reduction was 200 ml min^{-1} g^{-1}, and the reduction temperature was increased linearly from room temperature to 573 K over 4 h and maintained at 573 K for 2 h. Subsequently, the samples supporting the small Pt clusters were immersed in a 2.5×10^{-3} M aqueous solution of $Pt(NH_3)_4(NO_3)_2$ and the solution was evaporated in a rotary evaporator, in order to impregnate an additional amount of 5 wt% Pt. After subsequent drying of the samples in a vacuum oven at 320 K, the additionally impregnated Pt species was reduced by an H_2 flow. The reduction temperature was

increased linearly from room temperature to 673 K over 6 h and maintained there for 2 h.

The MCM-41 and KIT-1 samples with supported Pt were suspended in ethanol (99.9 vol.%). The suspension was dropped onto a porous carbon grid for TEM and allowed to dry in ambient atmosphere. TEM images were obtained from thin edges of the sample particles (<1 μm) with a CM 20 (Philips) apparatus operating at 100 keV.

The BET specific surface area S_{BET} for the samples was obtained using the standard BET method [24] for adsorption data in a relative pressure range from 0.06 to 0.25. The total surface area S_t, the primary mesopore surface area S_p, the external surface area S_{ex} and the primary mesopore volume V_p were obtained using the high-resolution α_s-plot method [25–28], in which LiChrospher Si-1000 silica gel ($S_{BET}=25$ m^2 g^{-1}) was used as a reference non-porous adsorbent. Note that in the current work, uniform mesopores of the materials under study are referred to as primary mesopores, whereas other mesopores present are called secondary mesopores. The external surface is defined as the surface of secondary mesopores and macropores, unless noted otherwise.

The α_s-plot method is based on an assumption that the course of adsorption in mesopores and macropores of an adsorbent under study is essentially the same as the course of adsorption for a non-porous reference adsorbent of similar surface properties (the similarity of surface properties is not crucial, when only multilayer adsorption data are used). In the α_s-plot method, the adsorption isotherm $v(p)$ (adsorption amount as a function of pressure p) for an adsorbent under study is expressed as a function of the adsorbed amount for the reference adsorbent. The required relation between pressure and the amount adsorbed for the reference solid is provided by its adsorption isotherm. Examples of the α_s-plots obtained can be seen in Figs. 1 - 3. Note that the adsorption for the reference adsorbent is written as the standard reduced adsorption: $\alpha_s=(v_{ref}(p))/v_{ref,\,0.4}$, where $v_{ref}(p)$ and $v_{ref,\,0.4}$ are the adsorbed amount for the reference solid as a function of pressure and the adsorbed amount at $p/p_0=0.4$ respectively. For many types of adsorbent the external (mesopore and macropore) surface area S_{ex} and the micropore volume V_{mi} can be obtained from high pressure adsorption data. Note, that according to the IUPAC recommendations, pores are classified as micropores (width below 2 nm), mesopores (width from 2 and 50 nm) and macropores (width above 50 nm) [29]. It is assumed that for α_s greater than

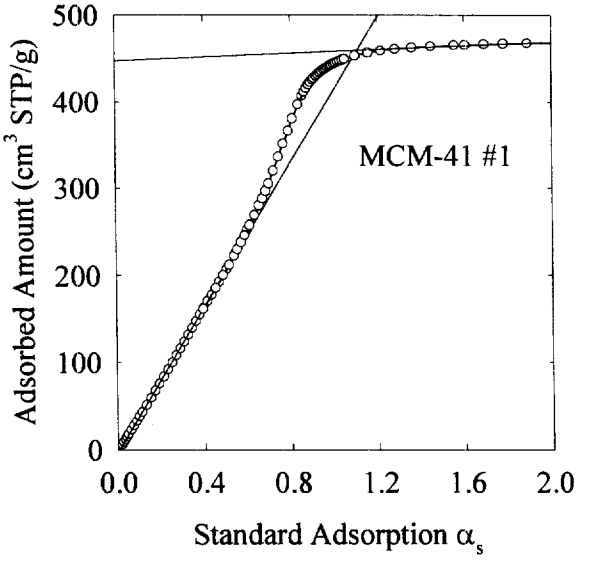

Fig. 1. The high-resolution α_s-plot for the #1 MCM-41 sample.

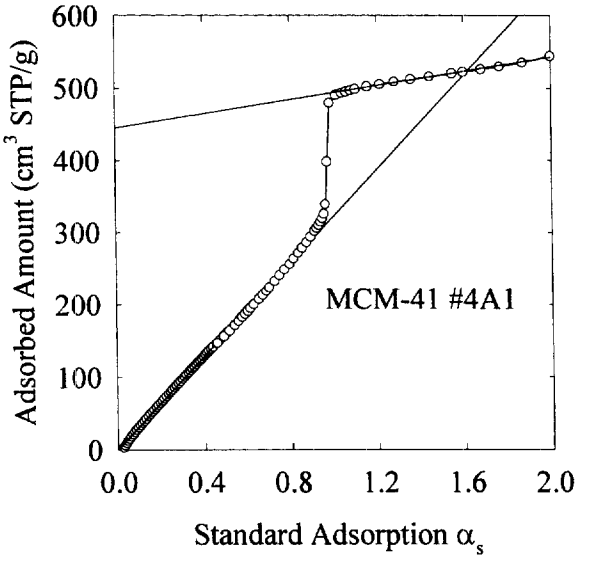

Fig. 2. The high-resolution α_s-plot for the #4A1 MCM-41 sample.

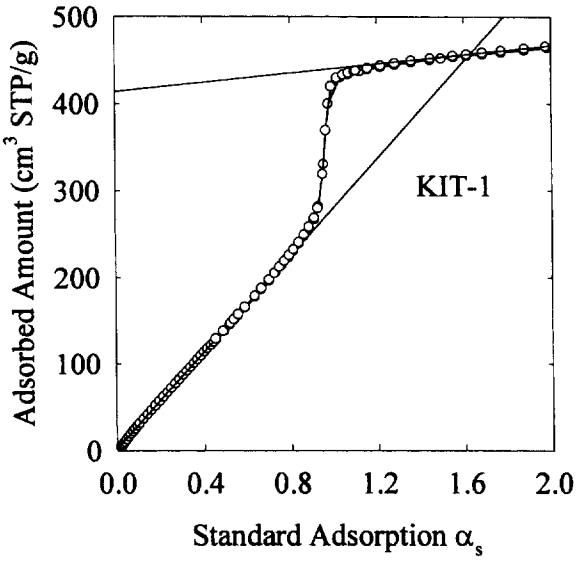

Fig. 3. The high-resolution α_s-plot for the KIT-1 sample.

ca. one ($p/p_0 > 0.4$), micropores (possibly present in a given sample) are completely filled and further increase in adsorption is due to the multilayer adsorption on the external surface of the sample. The latter adsorption process is assumed to proceed in the same way as a multilayer formation for the non-porous reference. Therefore, for $\alpha_s > 1$, a direct proportionality is expected between the adsorption on both the sample under study and the reference adsorbent, which would give rise to a linear part of the α_s-plot (provided there is no condensation in mesopores of the sample under study in a considered α_s interval):

$$v = v_{mi} + \eta\alpha_s \quad \text{for } \alpha_s > 1 \tag{1}$$

where η and v_{mi} are the slope and the intercept of the linear portion of the α_s-plot with the adsorbed amount axis. The intercept v_{mi} provides the amount adsorbed in micropores, which can be converted to the micropore volume $V_{mi} = c_f v_{mi}$, where c_f is a conversion factor between the volume of the gas and liquid adsorbate. For nitrogen adsorption at 77 K, c_f is equal to 0.0015468 for v_{mi}/cm^3 STP g^{-1} and V_{mi}/cm^3 g^{-1}. The slope η is related to the external (mesopore and macropore) surface area:

$$S_{ex} = \frac{\eta S_{BET,\,ref}}{v_{0.4,\,ref}}$$

where $S_{BET,\,ref}$ is the BET specific surface area for the reference adsorbent.

However, for ordered mesoporous materials, such as MCM-41 or KIT-1, the condensation in primary mesopores takes place for low α_s values, usually between 0.8 and 1.0, so the data for α_s below about 0.7 need to be used to assess the micropore volume v_{mi}:

$$v = v_{mi} + \eta_1\alpha_s \quad \text{for } \alpha_s < 0.7 \tag{2}$$

It needs to be noted that, in such a case, it is essential to use adsorption data (for both the reference solid and the material under study) measured starting from very low relative pressures. Moreover, the similarity of surface properties of these two materials is also crucial. As can be expected from previous studies of MCM-41 materials [18–21], the α_s-plot curves for the samples under the current study indicate the absence of microporosity, since initial parts of them are linear and approach origins of the plots (see Figs. 1–3). The slope η_1 of such a linear segment can be used to assess the total surface area

$$S_t = \frac{\eta_1 S_{BET,\,ref}}{v_{0.4,\,ref}}$$

Moreover, a higher pressure (α_s above ca. one) part of the α_s-plot can be used to obtain the external surface area (the surface area of secondary mesopores and macropores) S_{ex} and the volume of the primary mesopores V_p:

$$v = v_p + \eta_2\alpha_s \quad \text{for } \alpha_{s,pm} < \alpha_s < \alpha_{s,sm} \tag{3}$$

where η_2 and v_p are the slope and the intercept of the linear part of the plot in the high pressure region ($\alpha_s > \alpha_{s,pm}$) respectively. The lower limit of the α_s values, i.e. $\alpha_{s,pm}$, corresponds to the lowest pressure, for which the condensation of adsorbate in primary mesopores is already completed (usually, $\alpha_{s,p}$ equal to about 1.05 is suitable for most mesoporous molecular sieves, such as MCM-41). The upper limit, i.e. $\alpha_{s,sm}$, denotes the α_s value above which the capillary condensation in second-

ary mesopores takes place. The validity of the Eq. (3) rests upon the following assumptions: (i) after the condensation in the primary mesopores, the amount adsorbed in them does not change appreciably with further pressure increase; (ii) micropores are not present (which can be checked using the high resolution α_s-plot for low pressure data, as discussed above). The obtained v_p and η_2 are used to calculate the primary mesopore volume $V_p = c_f v_p$ (c_f was defined above) and the external (secondary mesopore and macropore) surface area:

$$S_{ex} = \frac{\eta_2 S_{BET,\,ref}}{v_{0.4,\,ref}}$$

When microporosity is not present, the difference between the total surface area S_t and the external surface area S_{ex} provides the primary mesopore surface area: $S_p = S_t - S_{ex}$.

The total pore volume V_t for the samples was estimated by multiplying the amount of nitrogen adsorbed at a relative pressure 0.99 by a conversion factor c_f between the volume of the gas and liquid adsorbate. The pore size distribution (PSD) was obtained from desorption data using the Barrett–Joyner–Halenda (BJH) method [30] implemented in the software provided with the ASAP 2010 adsorption apparatus. In the latter procedure, the Kelvin equation of the form $r/\mathrm{nm} = -0.953/\ln(p/p_0)$ was used and the statistical film thickness was represented by the Halsey equation ($t/\mathrm{nm} = 0.354[-5/\ln(p/p_0)]^{0.333}$).

The primary mesopore diameter w_d for the MCM-41 samples was calculated from the X-ray spacing d_{100} (later denoted as d) and the specific primary mesopore volume V_p according to the following relation [22,23,31]:

$$w_d = cd\left(\frac{\rho V_p}{1+\rho V_p}\right)^{1/2} \tag{4}$$

where $c = [8/(3^{1/2}\pi)]^{0.5} = 1.213$ and $\rho = 2.2\ \mathrm{g\ cm^{-3}}$ [23] is the density of pore walls. Eq. (4) holds for an infinite array of cylindrical pores arranged in a hexagonal pattern and, therefore, cannot be applied for the KIT-1 disordered material. However, for all samples, the primary mesopore diameter can be assessed approximately from the primary mesopore volume V_p and surface area S_p (under the assumption of cylindrical pore geometry) [18,23]: $w_{4V/S} = 4V_p/S_p$.

The pore wall thickness b_d for the MCM-41 samples was assessed from geometrical considerations as a difference between the distance between the pore centers a ($a = 2/(3^{1/2})d$) and the pore diameter w_d:

$$b_d = a - w_d = d\left[\frac{2}{3^{1/2}} - c\left(\frac{\rho V_p}{1+\rho V_p}\right)^{1/2}\right] \tag{5}$$

The calculations are based on the interplanar spacing d and the primary mesopore volume V_p. Note that most methods to evaluate the pore wall thickness from XRD and adsorption data involve a subtraction of two quantities of similar value (i.e. the pore center distance and pore diameter) with a certain absolute error, which may be comparable with the magnitude of the pore wall thickness to be calculated. Therefore, values of the latter vary significantly even for a series of samples of similar structural properties [22,23]. Moreover, the pore size is usually assessed on the basis of the Kelvin equation or the primary mesopore surface area, which may lead to quite significant errors. Therefore, the resulting pore wall thickness values are not only inconsistent, but may also be very inaccurate. However, the calculations of the pore wall thickness b_d from geometrical considerations (Eq. (5)) are affected by a relative (rather than absolute) error of the assessment of the interplanar spacing and do not require an independent method of pore size evaluation. Consequently, such calculations were shown to provide consistent (within ca. 0.1 nm) results for series of MCM-41 and HMS samples synthesized using similar methods [22,23] and, therefore, are suitable for comparative purposes, most likely providing also quite reliable estimates of the actual value of the pore wall thickness. A detailed discussion of methods to calculate the pore diameter and the pore wall thickness for MCM-41 materials can be found elsewhere [23].

Adsorption energy distributions [32] were calculated using the Integ program [33], which performs an inversion of the integral equation for the total adsorbed amount Θ_t with respect to the adsorption

energy distribution (AED) $F(\epsilon)$:

$$\Theta_t = \int_{\epsilon_{min}}^{\epsilon_{max}} \theta_l(\epsilon,p)F(\epsilon)\,d\epsilon \quad (6)$$

In Eq. (6), Θ_t is the total relative adsorption, $\theta_l(\epsilon,p)$ is a local adsorption isotherm, p is pressure and ϵ is the adsorption energy. The integration is carried out in an adsorption energy interval from ϵ_{min} to ϵ_{max}. To ensure the numerical stability of calculated AEDs, the Integ program employs the regularization method [33].

The total relative adsorption (later referred to as the relative adsorption) Θ_t can be estimated from the adsorption data according to the formula $\Theta_t(p) = v(p)/v_m$. In the current study, the monolayer capacity v_m was estimated from the total surface area S_t calculated from the α_s-plot method. The Fowler–Guggenheim (FG) adsorption isotherm (monolayer, localized adsorption with lateral interactions) was chosen to represent the local adsorption isotherm $\theta_l(\epsilon,p)$ and a pathwise topology of adsorption sites was assumed:

$$\theta_l(\epsilon,p) = \frac{Kp\exp(z\omega\theta_l/k_BT)}{1+Kp\exp(z\omega\theta_l/k_BT)} \quad (7)$$

where T is absolute temperature, k_B is the Boltzmann constant, z is the number of nearest neighbors of a molecule in the monolayer and ω is the interaction energy between two nearest neighbor molecules. The Langmuirian constant K is defined as $K = K^0\exp(\epsilon/k_BT)$, where K^0 can be expressed in terms of partition functions for the isolated molecule in the gas phase and adsorbed phase. In the current study, the interaction parameter $z\omega/k_B = 190$ K and the regularization parameter $\gamma = 10^{-4}$ were used. Owing to the choice of the local adsorption isotherm θ_l, only submonolayer adsorption data ($v(p) < v_m$) were used for calculations of AED. Practical aspects of applications of AEDs in studies of MCM-41 and HMS mesoporous molecular sieves and unmodified and modified silica gels were described in detail elsewhere [22,23,34–36].

3. Results and discussion

Shown in Fig. 4 are XRD spectra for selected samples. The d_{100}-spacing values (later denoted as d-values) are listed in Table 1. The spectrum for the #4A2 sample is very similar to that of #4A1 and, therefore, is omitted. As reported previously [12,13], the synthesis procedure applied for the sample #1 leads to materials of rather low degree of structural ordering. The pH adjustment significantly improves the structure of mesoporous molecular sieves under study, as can be seen from XRD patterns for calcined samples #2 and #3. The latter exhibit several pronounced peaks in their X-ray spectra. As reported previously, the application of the salt effect [16] in addition to the pH adjustment allows one to attain excellent long-range ordering and uniformity of porous structures

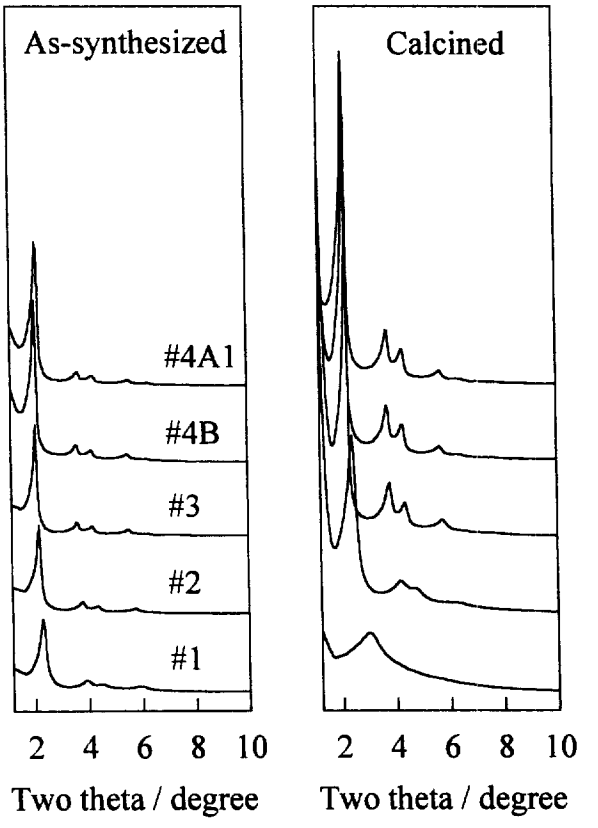

Fig. 4. The XRD spectra for selected MCM-41 mesoporous molecular sieves.

Table 1
Interplanar spacing, pore center distance and BET specific surface area for the samples

Sample	Interplanar spacing d_{100} (nm)	Pore center distance a (nm)	BET specific surface area S_{BET} ($m^2\ g^{-1}$)
#1	3.00	3.46	1420
#2	3.68	4.25	1240
#3	4.02	4.64	1060
#4A1	4.26	4.92	950
#4A2	4.15	4.79	860
#4B	4.11	4.75	950
KIT	4.20	N/A	840

and enhances remarkably the hydrothermal stability of the MCM-41 materials obtained (samples #4B, #4A1 and #4A2) [16]. It can be noticed that an application of the pH adjustment increased the d-spacing of the resulting materials: the sample #1 has $d=3$ nm, whereas #3 has $d=4.02$ nm.

The addition of Na_4EDTA at the early stage of the synthesis resulted in the formation of a material (denoted as KIT-1), which exhibits an XRD pattern similar to that of a lamellar phase [2] (see Fig. 5). However, not only was the structure of the mesoporous molecular sieve obtained retained after calcination, but it also showed an exceptional thermal and hydrothermal stability [14,15]. The

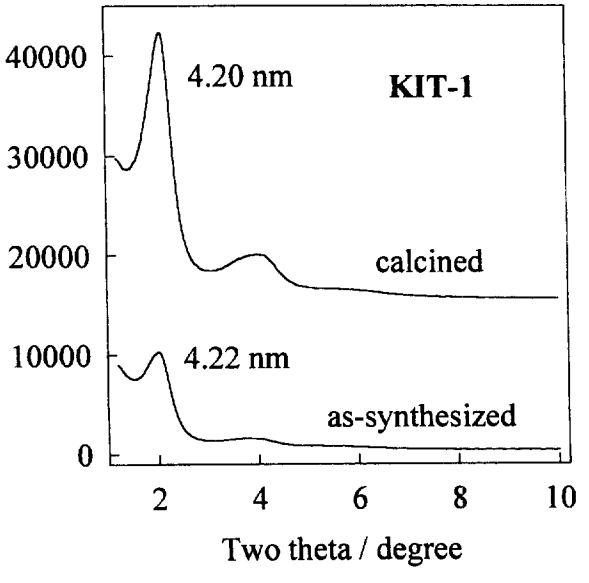

Fig. 5. The XRD spectra for the KIT-1 mesoporous molecular sieve.

observed XRD pattern may also be attributed to a disordered hexagonal structure similar to the MCM-41. Using a combination of several experimental techniques, the structure of the material was identified as a disordered network of worm-like interconnected channels exhibiting a very high degree of pore size uniformity [14–16].

TEM images obtained from microparticles of KIT-1 and MCM-41 are presented in Fig. 6. The TEM image for MCM-41 shows the hexagonal structure. However, no structural order can be noticed in the TEM image for KIT-1. The disordered TEM image for KIT-1 is similar to TEM images for disordered bicontinuous structures found in surfactant solutions. Since such a disordered TEM image comes from superposition of many channels, it is difficult to distinguish local structure of the disordered material. In particular, it is difficult to distinguish if three-dimensionally branched channels are interconnected, or one-dimensional channels of uniform diameter are entangled. The local structure of the channel arrangement in the disordered material can be probed by a TEM imaging technique using the platinum wires incorporated within pores, as reported recently [17]. The size and the number of the Pt wires have been controlled in order to obtain the channel images without superposition. The TEM images for KIT-1 and MCM-41 thus obtained are also presented in Fig. 6. The TEM images show that the KIT-1 particle contains a large number of short channels which are interconnected in a three-dimensional disordered way, whereas the MCM-41 channels are linear. Thus, the difference in channel connectivity is a conspicu-

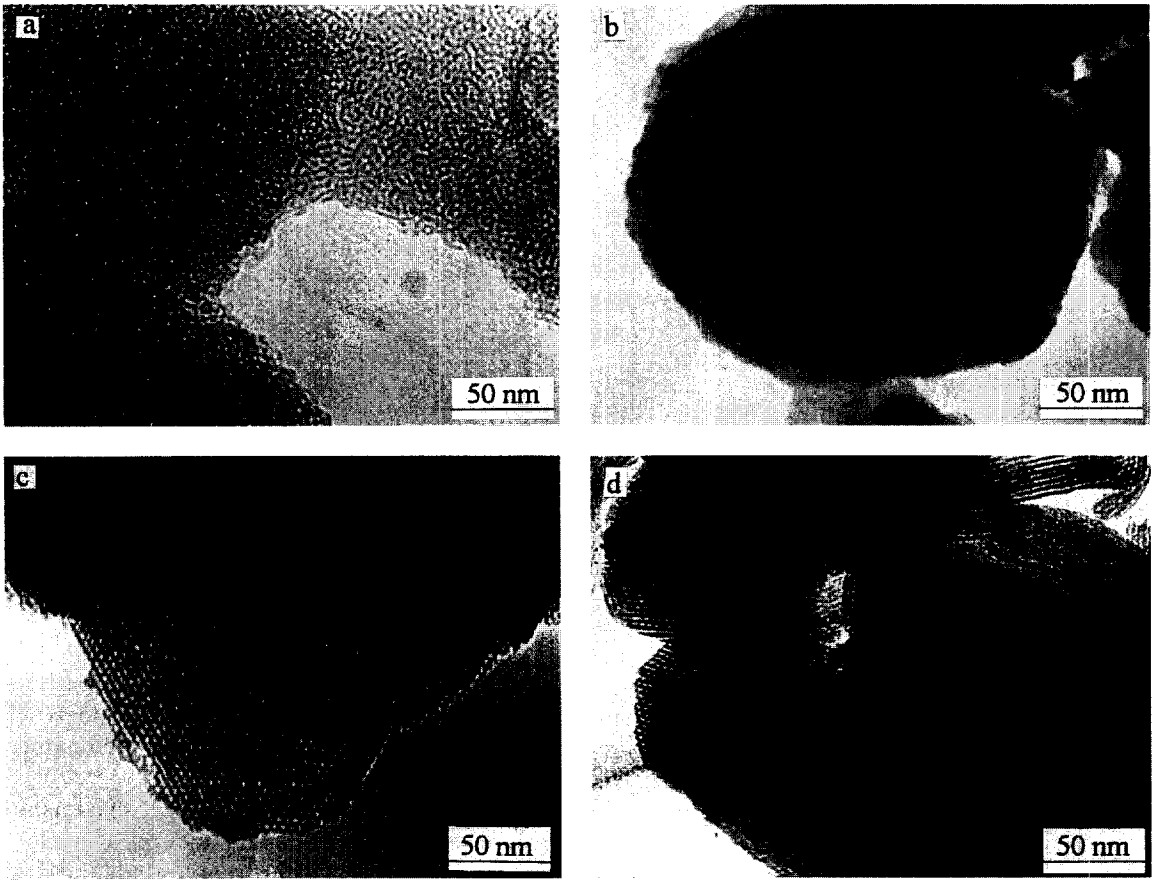

Fig. 6. Transmission electron micrographs: (a) calcined KIT-1, (b) KIT-1 after incorporating Pt wires, (c) calcined MCM-41, (d) MCM-41 after incorporating Pt wires.

ous difference between the two mesoporous materials.

Nitrogen adsorption isotherms for the samples under study are shown in Figs. 7–9. One can notice in Fig. 7 that the sharpness of the step of nitrogen condensation in primary mesopores increases significantly with the applied pH adjustment. For the sample #1, such a step is very broad and not well-pronounced. The adsorbed amount rises gradually until the relative pressure of about 0.4 is reached. Then, there is no appreciable increase in adsorption. Such a behavior indicates that the sample has a broad PSD in the pore size range up to about 4 nm and essentially no bigger mesopores. The latter conclusion can be drawn by comparing the adsorption isotherm for the sample #1 with isotherms for samples of uniform porous structures. It was shown (Ref. [23] and the current study) that the condensation in 4 nm cylindrical pores takes place at p/p_0 close to 0.4.

In the case of the sample #2, the step of the nitrogen condensation in primary mesopores is pronounced, but quite broad, whereas for other materials, such steps are sharp, especially for the #4B, #4A1 and #4A2 samples. The presence of a narrow step for KIT-1 proves that its PSD is highly monodispersive. On the basis of previous studies of ordered mesoporous molecular sieves [6,37], it can be expected that if the KIT-1 had an ordered structure of such uniform pore size, there would be a very clear XRD pattern reflecting the structure of the material. Note for example that

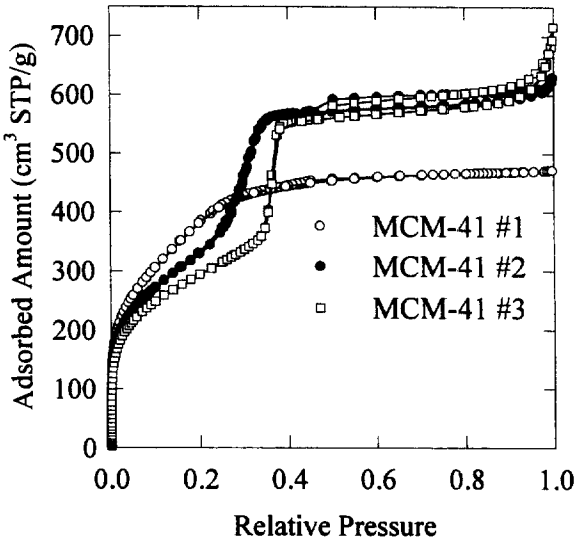

Fig. 7. Nitrogen adsorption isotherms for #1, #2 and #3 MCM-41 samples.

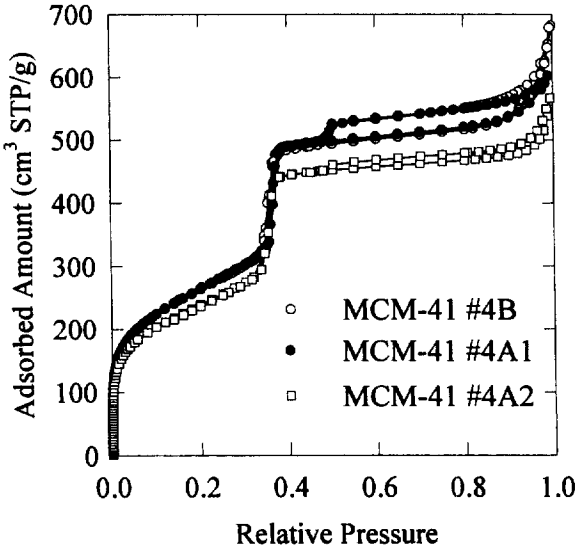

Fig. 8. Nitrogen adsorption isotherms for #4B, #4A1 and #4A2 MCM-41 samples.

the sample #2 has a broader condensation step on its adsorption isotherm (Fig. 7), but yet at least four peaks can be identified on its XRD spectrum (see Fig. 4). In contrary to that, the XRD pattern for the KIT-1 (Fig. 5) shows just two (or possibly three, but the last one is not well-pronounced)

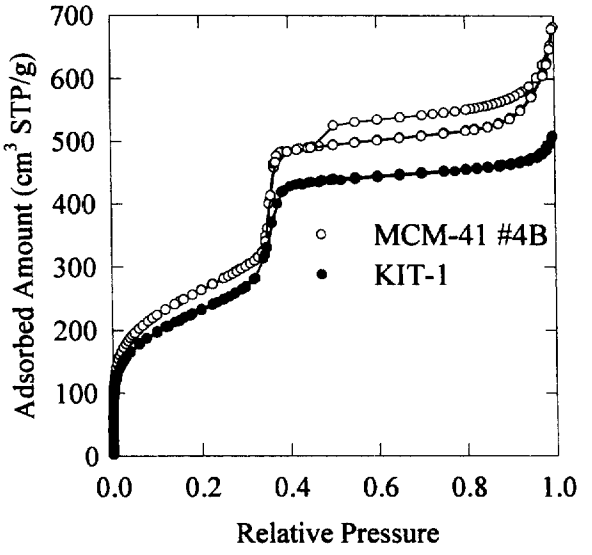

Fig. 9. Nitrogen adsorption isotherms for #4B MCM-41 and KIT-1 samples.

rather broad peaks. Therefore, the comparison of the nitrogen adsorption and XRD data is additional strong evidence for the disordered nature of the KIT-1 material.

As can be seen in Fig. 7, the pH adjustment led to an increase of secondary mesoporosity of the samples, which is evident from a gradual development of a high-pressure hysteresis loop for $p/p_0 > 0.85$. Moreover, there is a marked decrease in the BET specific surface area (see Table 1). It needs to be noted that the synthesis of good quality MCM-41 samples using the pH adjustment and the salt effect is highly reproducible and provides materials with essentially the same porous structures, as evident from almost identical shapes of their nitrogen adsorption isotherms (see Fig. 8).

In order to examine low pressure nitrogen adsorption for the samples under study, their isotherms were expressed as relative adsorption curves. As can be seen in Fig. 10, the course of low pressure adsorption for MCM-41 and KIT-1 materials is very similar, which can be expected, because both samples are siliceous in nature. It was already shown [23] that there is no noticeable difference between low pressure nitrogen adsorption for mesoporous silicas and MCM-41 molecular sieves. The results reported in the current study

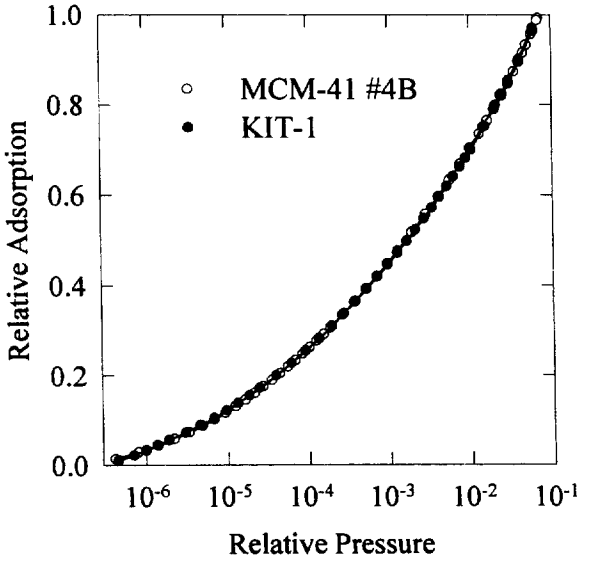

Fig. 10. Relative adsorption curves for #4B MCM-41 and KIT-1 samples shown in a logarithmic scale.

provide additional evidence that the surface properties of mesoporous siliceous molecular sieves are not influenced appreciably by details of morphology of porous structures of these materials.

Shown in Figs. 1–3 are high-resolution α_s-plots for selected molecular sieves under study. It can be noticed that the initial parts of the α_s-plot curves are linear and start from the origin of the graphs; this shows the lack of microporosity and proves the high similarity of surface properties (with respect to nitrogen) of the materials under study and porous silica gels, as the latter type of adsorbent was chosen as a reference material. The slopes of these initial parts of the α_s-plots were used to calculate the total surface area S_t for the samples (see Table 2). For most of the materials, the S_t obtained is in good agreement with the calculated BET specific surface area S_{BET} listed in Table 1. However, in the case of the sample #1, the BET method is inherently unable to provide a correct value of the surface area (at least in a classical BET pressure range from 0.05 to 0.3), since nitrogen condensation in smaller primary mesopores of the sample takes place in the BET pressure region. This can be clearly seen from the α_s-plot for sample #1 (see Fig. 1), as deviations from linearity of the initial part of the plot (caused by the condensation in mesopores) appear for α_s as low as ca. 0.6, which corresponds to a relative pressure of about 0.05. Owing to the nitrogen condensation in the pores in the BET pressure region, the S_{BET} value for sample #1 is a serious overestimation of the actual specific surface area. Therefore, the assessment of the specific surface area for mesoporous materials with a significant fraction of mesopores below ca. 3 nm, and especially those close to 2 nm, cannot be performed reliably using the standard BET method (as already suggested in Ref. [23]). In such cases, the application of comparative methods, such as the α_s-plot or t-plot, is recommended.

The primary mesopore volume V_p and the external surface area S_{ex} for the samples were assessed on the basis of high-pressure adsorption data (α_s from 1.1 to 1.7 for sample #1, from 1.3 to 2.0 for KIT-1 and from 1.05 to 1.7 for all other materials). As can be seen from Table 2, the application of a single pH adjustment for #2 MCM-41 caused an increase in its V_p. However, the repeated pH adjustment led to a slight decrease in the primary mesopore volume, as can be inferred by comparing data for #2 and 3# MCM-41 samples. Moreover, the addition of Na_4EDTA after the first pH adjustment caused a significant lowering of V_p.

Primary mesopore surface areas S_p listed in Table 2 were calculated from the corresponding S_t and S_{ex} values: $S_p = S_t - S_{ex}$. It can be seen that S_p values decrease when the pH adjustment is applied and a further lowering of S_p is brought by the application of the salt effect. The primary mesopore surface areas S_p and volumes V_p were used to calculate the pore diameter for the samples under study from the formula $w_{4V/S} = 4V_p/S_p$. The pore diameter was also assessed, probably much more accurately [23], using d-spacing from XRD and the primary mesopore volume V_p. Eq. (4) was applied in these calculations. The resulting pore diameters w_d are listed in Table 3. The relative pressures p_c/p_0 of inflection points on nitrogen condensation steps in primary mesopores of the samples are also provided. One can notice an excellent correlation between the p_c/p_0 values and w_d values obtained in the current study as well as

Table 2
Structural parameters obtained from high resolution from the α_s-plot method for the samples under study

Sample	Total surface area ($m^2\,g^{-1}$)	External surface area ($m^2\,g^{-1}$)	Primary mesopore surface area ($m^2\,g^{-1}$)	Primary mesopore volume ($cm^3\,g^{-1}$)	Total pore volume ($cm^3\,g^{-1}$)
#1	1200	40	1160	0.68	0.73
#2	1150	80	1070	0.84	0.95
#3	1030	120	910	0.80	1.04
#4A1	930	140	790	0.69	0.93
#4A2	830	100	730	0.64	0.84
#4B	910	140	770	0.68	1.01
KIT	800	80	720	0.64	0.77

Table 3
Relative pressure of nitrogen condensation in primary mesopores, pore diameter and pore wall thickness for the samples

Sample	Relative pressure of nitrogen condensation p_c/p_0	Pore width[a] w_d (nm)	Pore wall thickness b_d (nm)	Pore width $w_{4V/S}$ (nm)
#1	—	2.82	0.64	2.36
#2	0.31	3.60	0.65	3.14
#3	0.36	3.89	0.75	3.52
#4A1	0.36	4.01	0.91	3.48
#4A2	0.36	3.85	0.94	3.54
#4B	0.35	3.86	0.89	3.55
KIT	0.35	N/A	N/A	3.52

[a] Calculated from XRD d-spacing and primary mesopore volume using Eq. (4).

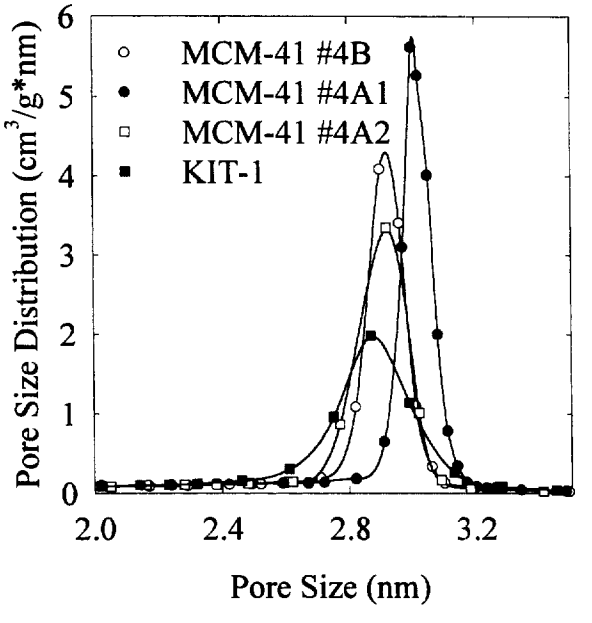

Fig. 11. BJH PSD for #4B, #4A1, #4A2 MCM-41 and KIT-1 samples.

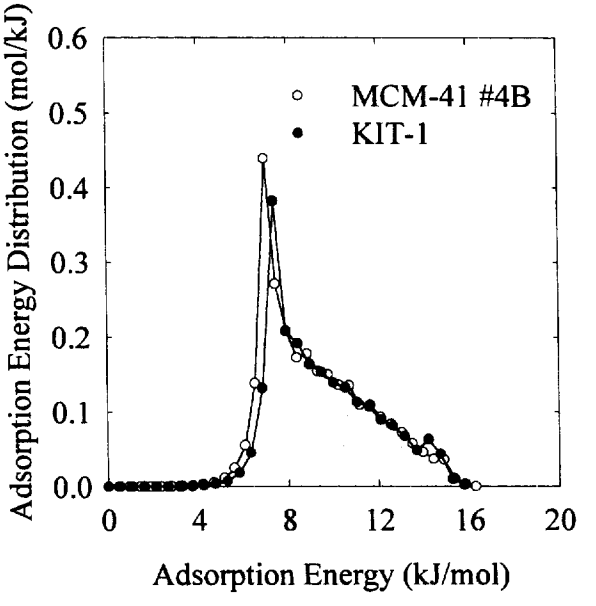

Fig. 12. AEDs for #4B MCM-41 and KIT-1 samples.

in our previous work [23]. The relative pressure of the condensation step (p_c/p_0) increases as the pore diameter w_d increases, even in cases when the difference in w_d values for the compared samples are very small. On the basis of the data from Table 3, the pore size for the KIT-1 sample can be estimated as about 3.9 nm, as the nitrogen condensation step for the disordered molecular sieve appears for pressure very close to that for the condensation step on the isotherm for the #4B sample, which has $w_d = 3.86$ nm.

The pore wall thickness was assessed from the XRD d-spacing and the primary mesopore volume V_p on the basis of the geometrical considerations (Eq. (5)). It can be seen from Table 3 that the repeated pH adjustment gave rise to materials of somewhat thicker pore walls than in the case when the pH adjustment was not applied. The salt effect caused a significant further increase in the thickness of pore walls. The above findings provide a reason (or more likely one of several reasons) for the significantly higher thermal and hydrothermal stability of materials synthesized using both the pH adjustment and the salt effect.

BJH PSDs calculated from desorption data for selected samples are shown in Fig. 11. It can be noticed that the peaks on these distributions are very sharp, indicating a high uniformity of porous structures of the mesoporous molecular sieves obtained using the repeated pH adjustment. Note that the BJH PSD for the KIT-1 is somewhat broader, which may possibly result from one or both of the following factors: (i) broader range of pore sizes, and (ii) pore shape heterogeneity caused by the presence of curved worm-like pores. It can be seen that maxima on the BJH PSDs appear for pore diameter values significantly smaller than those calculated from XRD and adsorption data through Eq. (4). Similar differences were reported previously [23] and attributed to an underestimation of pore diameters using the BJH method.

AEDs for the #4B MCM-41 and KIT-1 samples are shown in Fig. 12. The AEDs lie in an adsorption energy interval from about 5 to 16 kJ mol^{-1} and feature a pronounced peak at ca. 7 kJ mol^{-1}. Then, they decline gradually. They are similar to one another and to AEDs previously reported for other MCM-41 samples [23].

4. Conclusions

A combination of the XRD, TEM and adsorption techniques is a very powerful tool for characterization of mesoporous molecular sieves. This allows one to obtain information about the morphology of porous structures, the PSD, the surface area and the surface properties of the materials. In the current study, the XRD, TEM and nitrogen adsorption were used successfully to monitor structures of mesoporous molecular sieves synthesized hydrothermally and tailored using the pH adjustment and the salt effect. It was shown that the repeated pH adjustment remarkably improves the uniformity of pores of MCM-41 materials. The application of the salt effect after the first pH adjustment increased the thickness of pore walls of the samples, which may explain their exceptional thermal and hydrothermal stability reported previously. The synthesis procedure for the latter high quality MCM-41 materials appeared to be highly reproducible. It was shown that although the KIT-1 exhibits a remarkable pore size uniformity, it has a rather featureless XRD spectrum. These findings strongly support a previous identification of the material as a disordered mesoporous molecular sieve.

The application of comparative plots appears to be promising in the characterization of new mesoporous materials. It may be advantageous over the standard BET method in the assessment of the specific surface area, especially for samples possessing small mesopores (diameter below ca. 3 nm). Moreover, the comparative methods allow for an estimation of the external surface area, the primary mesopore area and primary mesopore volume, the latter being useful for calculations of primary mesopore diameter for MCM-41, especially when X-ray data are also available. The comparative plots can also provide evidence for the absence (or presence) of microporosity. Low surface area silica gels can conveniently serve as reference adsorbents, since low pressure nitrogen adsorption appeared to be rather insensitive to details of mesopore structure morphology.

References

[1] C.T. Kresge, M.E. Leonowicz, W.J. Roth, J.C. Vartuli, J.S. Beck, Nature 359 (1992) 710.

[2] J.S. Beck, J.C. Vartuli, W.J. Roth, M.E. Leonowicz, C.T. Kresge, K.D. Schmitt, C.T.-W. Chu, D.H. Olson, E.W. Sheppard, S.B. McCullen, J.B. Higgins, J.L. Schlenker, J. Am. Chem. Soc. 114 (1992) 10834.
[3] C.-Y. Chen, H.-X. Li, M.E. Davis, Microporous Mater. 2 (1993) 17.
[4] C.-Y. Chen, S.L. Burkett, H.-X. Li, M.E. Davis, Microporous Mater. 2 (1993) 27.
[5] A. Monnier, F. Schuth, Q. Huo, D. Kumar, D. Margolese, R.S. Maxwell, G.D. Stucky, M. Krishnamurty, P. Petroff, A. Firouzi, M. Janicke, B.F. Chmelka, Science 261 (1993) 1299.
[6] Q. Huo, D.I. Margolese, U. Ciesla, P. Feng, T.E. Gier, P. Sieger, R. Leon, P.M. Petroff, F. Shüth, G.D. Stucky, Chem. Mater. 6 (1994) 1176.
[7] P.T. Tanev, T.J. Pinnavaia, Science 267 (1995) 865.
[8] Q. Huo, D.I. Margolese, G.D. Stucky, Chem. Mater. 8 (1996) 1147.
[9] N.K. Raman, M.T. Anderson, C.J. Brinker, Chem. Mater. 8 (1996) 1682.
[10] A. Sayari, in: H. Chon, S.I. Woo, S.-E. Park (Eds.), Recent Advances and New Horizons in Zeolite Science and Technology, Elsevier, Amsterdam, 1996, p. 1.
[11] A. Sayari, Chem. Mater. 8 (1996) 1840.
[12] J.M. Kim, J.H. Kwak, S. Jun, R. Ryoo, J. Phys. Chem. 99 (1995) 16742.
[13] R. Ryoo, J.M. Kim, J. Chem. Soc. Chem. Commun. (1995) 711.
[14] R. Ryoo, J.M. Kim, C.H. Shin, J.Y. Lee, in: H. Chon et al. (Eds.), Progress in Zeolites and Microporous Materials, Studies in Surface Science and Catalysis, vol. 101, Elsevier, Amsterdam, 1997, p. 45.
[15] R. Ryoo, J.M. Kim, C.H. Ko, C.H. Shin, J. Phys. Chem. 100 (1996) 17718.
[16] R. Ryoo, S. Jun, J. Phys. Chem. B 101 (1997) 317.
[17] C.H. Ko, R. Ryoo, J. Chem. Soc. Chem. Commun. (1996) 2467.
[18] O. Franke, G. Schulz-Ekloff, J. Rathousky, A. Zukal, J. Chem. Soc. Chem. Commun. (1993) 724.
[19] P.J. Branton, P.G. Hall, K.S.W. Sing, J. Chem. Soc. Chem. Commun. (1993) 1257.
[20] J. Rathousky, A. Zukal, O. Franke, G. Schulz-Ekloff, J. Chem. Soc. Faraday Trans. 90 (1994) 2821.
[21] P.J. Branton, P.G. Hall, K.S.W. Sing, H. Reichert, F. Schuth, K.K. Unger, J. Chem. Soc. Faraday. Trans. 90 (1994) 2965.
[22] M. Kruk, M. Jaroniec, A. Sayari, Microporous Mater. 9 (1997) 173.
[23] M. Kruk, M. Jaroniec, A. Sayari, J. Phys. Chem. B 101 (1997) 583.
[24] S. Brunauer, P.H. Emmett, E. Teller, J. Am. Chem. Soc. 60 (1938) 309.
[25] M. Jaroniec, in: T.J. Pinnavaia, M.F. Thorpe (Eds.), Access to Nanoporous Materials, Plenum, New York, 1996, p. 255.
[26] S.J. Gregg, K.S.W. Sing, Adsorption, Surface Area and Porosity, Academic Press, London, 1982.
[27] K. Kaneko, C. Ishii, M. Ruike, H. Kuwabara, Carbon 30 (1992) 1075.
[28] M. Kruk, M. Jaroniec, J. Choma, submitted to Carbon.
[29] K.S.W. Sing, D.H. Everett, R.A.W. Haul, L. Moscou, R.A. Pierotti, J. Rouquerol, T. Siemieniewska, Pure Appl. Chem. 57 (1985) 603.
[30] E.P. Barrett, L.G. Joyner, P.P. Halenda, J. Am. Chem. Soc. 73 (1951) 373.
[31] T. Dabadie, A. Ayral, C. Guizard, L. Cot, P. Lacan, J. Mater. Chem. 6 (1996) 1789.
[32] M. Jaroniec, R. Madey, Physical Adsorption on Heterogeneous Solids, Elsevier, Amsterdam, 1988.
[33] M. von Szombathely, P. Brauer, M. Jaroniec, J. Comput. Chem. 13 (1992) 17.
[34] Y. Bereznitski, M. Jaroniec, M. Kruk, J. Liq. Chromatogr. 19 (1996) 1523.
[35] Y. Bereznitski, M. Jaroniec, M. Kruk, B. Buszewski, J. Liq. Chromatogr. 19 (1996) 2767.
[36] M. Kruk, M. Jaroniec, R.K. Gilpin, Y.W. Zhou, Langmuir 13 (1997) 545.
[37] Q. Huo, R. Leon, P.M. Petroff, G.D. Stucky, Science 268 (1995) 1324.